Journal of Hazardous Materials 420 (2021) 126612

Contents lists available at ScienceDirect

Journal of Hazardous Materials

journal homepage: www.elsevier.com/locate/jhazmat

Research Paper

Arsenopyrite weathering in acid rain: Arsenic transfer and environmental implications

Xiaonan Feng [a,b], Qingyou Liu [a,*], Shuai Wang [a,b], Ling Cen [a,b], Heping Li [a,*]

[a] Key Laboratory of High-temperature and High-pressure Study of the Earth's Interior, Institute of Geochemistry, Chinese Academy of Sciences, Guiyang 550081, China
[b] University of Chinese Academy of Sciences, Beijing 100039, China

ARTICLE INFO

Editor: Dr. L. Haizhou

Keywords:
Arsenopyrite
Acid rain
Electrochemical technique
Surface analysis
Arsenic transform

ABSTRACT

Arsenopyrite is widely distributed and weathers readily in the nature, releases As and pollutes the surrounding environment. Acid rain is acidic in nature as contains sulfur oxides (SO_x) and nitrogen oxides (NO_x), and is a typical hazardous material to human. When arsenopyrite encounters acid rain, their interaction effect may aggregate environmental degradation. In this work, the weathering behavior of arsenopyrite in simulated acid rain was studied using the electrochemical techniques and surface analysis. Cyclic voltammetry and Raman and XPS confirmed that FeAsS was oxidized to Fe^{2+}, AsO_3^{3-} and S^0 at the initial phase, then, Fe^{2+} was converted to Fe^{3+}, S^0 transformed to SO_3^{2-} and ultimately to SO_4^{2-}, and AsO_3^{3-} to AsO_4^{3-} with the accumulation of H^+. Polarization curve revealed higher temperature or higher acidity of acid rain increased the weathering trend and rate of arsenopyrite, and electrochemical impedance spectroscopic measurements showed the causes behind this to be smaller resistance and greater capacitance at the double layer and passivation film. Arsenopyrite weathering rate and temperature has a relationship: $\ln k = -3824.8/T + 10.305$, via a transition state with activation enthalpy 29.37 kJ mol^{-1} and activation entropy − 167.40 J mol^{-1} K^{-1}. This study provides a rapid and quantitative in-situ electrochemical method for arsenopyrite weathering and an improved understanding of arsenopyrite weathering in acid rain condition. The results have powerful implications for the remediation and management of As-bearing sites affected by mining activities in acid rain area.

1. Introduction

Arsenopyrite (FeAsS) is the most abundant and ubiquitous mineral containing arsenic on the earth (Deng and Gu, 2018). Decomposition of arsenopyrite due to the oxidation by oxygen present in the air of natural environment leads to the release of large quantity of arsenite (AsO_3^{2-}), arsenate (AsO_4^{2-}) and sulfate (SO_4^{2-}) into the surrounding environment. These species are responsible for hazardous arsenic pollution as well as acid mine drainage (AMD), leading to ecosystem disorders and even affecting the human health (Coussy et al., 2011; Zhang et al., 2020a, 2020b). According to the World Health Organization, uptake of 10 μg L^{-1} arsenic by the human body will lead to arsenic poisoning. Long-term human intake/exposure to arsenic-containing foods/environments can lead to chronic poisoning resulting to abdominal pain, diarrhea, vomiting, and even cancer and death. Conservative estimation has given a figure of about 140 million people who might at risk of arsenic poisoning (Glodowska et al., 2020; Silva et al., 2020). Additionally, arsenopyrite is also often associated to chalcopyrite (CuFeS), sphalerite (ZnS), galena (PbS) and others, which led to the release of other heavy metal elements including Pb and Cu apart from As due to oxidation and thus intensifying the environmental hazards (Lizaro et al., 1997). It has been proved that electrochemical process is responsible for the release of arsenic from arsenopyrite. Liu et al. (2020) used electrochemical analytical methods to confirm that arsenopyrite released arsenic through electrochemical reaction in acidic iron free 9 K medium. Walker et al. (2006) demonstrated that the release of arsenic was in the forms of arsenate and arsenite, and sulfur was released as sulfate when arsenopyrite was oxidized by dissolved oxygen. Some works have proven that the oxidation of arsenopyrite is strongly controlled by the concentration of dissolved Fe(III), especially at acidic pH (Yu et al., 2007).

Acid rain or acidic deposition includes wet deposition (rain, snow and fog) and dry deposition (acid gases and particles) (Moldovan et al., 2014). The excessive presence of sulfur oxides (SO_x) and nitrogen oxides (NO_x) in the atmosphere caused by carbon combustion, industrial development, motor vehicle emissions and others sources dissolve into rainwater and get further converted into sulfuric acid and nitric acid,

* Corresponding authors.
E-mail addresses: liuqingyou@vip.gyig.ac.cn (Q. Liu), liheping@vip.gyig.ac.cn (H. Li).

https://doi.org/10.1016/j.jhazmat.2021.126612
Received 6 March 2021; Received in revised form 5 July 2021; Accepted 7 July 2021
Available online 8 July 2021

and thus aggravates the formation of acid rain (Li et al., 2018; Wang et al., 2000). Acid rain has been one of the serious air pollution and has attracted worldwide attention. Acid rain results in forest decline, soil acidification, buildings damage and increases the solubility and migration of heavy metal contaminant and the acidity of surface water and groundwater, and even causes ecological disturbance and further endanger human health (Cui et al., 2014a, 2014b; Larssen et al., 2000). Various studies have revealed rapid increase of the areas eroded by acid rain and the acidity of precipitation (Zhang et al., 2017), therefore, it is very important to understand the effect of acid rain or other global climate change on environmental pollution (Nordstrom, 2009).

As arsenopyrite is characterized with semiconductor property, arsenopyrite weathering is bound to occur when encounter with acid rain, and thereby releasing arsenic and changing the acidity of the rainfall. The previous studies (Hammond et al., 2020; Silva et al., 2020) have confirmed that rainfall caused migration of the arsenopyrite tailings to a wider range under the rain erosion, resulting in serious environmental issue. In nature, arsenopyrite weathering is an electrochemical process. Many researchers have used electrochemical techniques to study the oxidation of arsenopyrite under different electrolytes (Lin and Zheng, 1996; Kostina and Chernyak, 1979a, 1979b), different acidities (Deng et al., 2018; Lazaro et al., 1997) or basicities (Hiskey and Sanchez, 1987; Sanchez and Hiskey, 1988), even presence of microorganism (Liu et al., 2020; Zeman et al., 1995). To the best of our knowledge, there is no report concerning arsenopyrite weathering in acid rain from electrochemical view. Therefore, in this study, different electrochemical and surface analysis measurements were conducted to investigate the weathering behavior of arsenopyrite in simulated acid rain (SAR) solutions at different temperatures and acidities, with the following purposes: (1) to understand arsenopyrite weathering trend under different acid rain conditions; (2) to quantitatively obtain arsenopyrite weathering rate, especially the release rate of arsenic; (3) to specify the inorganic arsenic speciation during the transformation process of arsenopyrite weathering, and (4) ultimately reveal arsenopyrite weathering mechanism, and provide theoretical basis for the remediation and management of As-bearing sites in acid rain area affected by mining activities.

2. Materials and methods

2.1. Arsenopyrite specimens and simulated acid rain preparation

The arsenopyrite samples collected in this experiment came from the Carlin-type gold deposit in Guangxi Province, South China. X-ray diffraction (Empyrean, Panaco of Netherlands) indicated that the minerals were pure and homogeneous (Fig. S1). Electron microprobe (JXA-8230, JEOL) was used to further analyze the elemental composition of the minerals and showed that it was mainly consisting of 46.10% As, 33.58% Fe, and 19.23% S (wt%) (Table S1), indicating that the samples used in this experiment were close to the theoretical arsenopyrite composition.

On one hand, pure arsenopyrite samples were used for the electrode preparation. Specifically, the sample was firstly cut into cube with a dimension of about 0.7 × 0.7 × 0.9 cm^3, then, placed in a fabricated mold. Next, a copper wire was connected to the upper surface using silver-loaded conductor and finally sealed with epoxy resin to expose only the lower surface in contact with the electrolyte to work as the working electrode. The detailed and specific electrode fabrication method was shown by MuñOz et al. (1998). On the other hand, rest of the samples were crushed, selected, and grounded into powder of about 200 meshes (~74 μm) for the immersion experiments.

The SAR solutions were prepared based on the monitoring data of Dongchuan Environmental Monitoring Station (An, 2015). The chemical composition was: 0.0138 g L^{-1} $CaSO_4$, 0.0048 g L^{-1} $(NH_4)_2SO_4$, 0.0049 g L^{-1} $MgSO_4$, 0.0034 g L^{-1} $NaNO_3$, 0.0004 g L^{-1} NH_4Cl, 0.0005 g L^{-1} NaCl and 0.0015 g L^{-1} KF. The SO_4^{2-}:NO_3^- = 3.39:1(molar ratio), and hence H_2SO_4 + HNO_3 (molar ratio, 3.39:1) and NaOH solutions were used to obtain pH 3.6, pH 4.6, and pH 5.6.

2.2. Electrochemical measurements

An electrochemical workstation (PARSTAT 2273) combined with a computer was used to conduct all the electrochemical experiments using a traditional three-electrode system including working electrode (arsenopyrite electrode), auxiliary electrode (platinum electrode) and reference electrode (saturated calomel electrode (SCE)). They were immersed in about 30 mL solution to adjust different experimental temperatures via a constant temperature water bath. All the potentials reported in this study are relative to the SCE (0.245 V versus standard hydrogen electrode at 25 °C).

The electrochemical measurements mainly include open circuit potential (OCP), cyclic voltammetry (CV), polarization curve and electrochemical impedance spectroscopy (EIS). Before each electrochemical test, the OCP was measured to reach a quasi-steady state (< 2 mV per 5 min and keep 400 s) to ensure the stability and reproducibility. The CV measurement was performed form OCP to 0.7 V (vs. SCE), and then reversed to 1.0 V, finally back to OCP at 10 mV s^{-1} rate. For polarization curve it was scanned from - 0.25 V to + 0.25 V (vs. OCP) at 10 mV S^{-1} rate. The EIS was carried out at OCP in the frequency region of 10^{-3}–10^5 Hz with amplitude of 10 mV. ZSimpWin and PowerSuit softwares were used to fit the impedance and polarization data. To ensure reproducibility, at least three experiments were performed and the average results are reported in this study.

2.3. Batch soaking experiments and characterization

Arsenopyrite powder samples having mesh size of about 200 (~74 μm), were used for Raman and X-ray photoelectron spectroscopy (XPS) analysis. The samples were divided into seven different groups. One was pristine sample without any treatment, while the other six were soaked in different solutions: (1) 5 °C, pH 4.6; (2) 15 °C, pH 4.6; (3) 25 °C, pH 4.6; (4) 35 °C, pH 4.6; (5) 25 °C, pH 3.6; (6) 25 °C, pH 5.6. In an Erlenmeyer flask having 100 mL volume, 0.5 g powder and 50 mL corresponding solution were added and weathered for two months under different conditions. After two months, one pristine sample and six eroded samples taken out from six different weathering conditions were characterized by Raman and XPS. Raman spectra was measured by a British Renishaw instrument at 50 mW (5%) laser power, 30 s laser time and 514 nm wavelength in order to prevent damage of the sample surface by laser. XPS (ESCALAB 250XI) was used to characterize the chemical states of As, S and Fe in the samples. The Avantage 5.948 and XPSPEAK41 software were used to fit and analyze the related chemical states distributions and elemental contents (at%) data corrected by the C1s peak at 284.8 eV. As *3d* and S *2p* spectra were fitted by doublets with the same full width at half maximum and intensity ratios of 3:2 and 2:1 and spin-orbit splitting of 0.69 eV and 1.18 eV, respectively. Fe *2p* spectra was fitted by the theoretical core p level multiplet structures for free transition metal ions (GS multiplets) (Gupta and Sen, 1974, 1975).

3. Results and discussion

3.1. Electrochemical analysis: effect of temperature and acidity on arsenopyrite weathering tendency

3.1.1. Open circuit potential

Open circuit potential refers to the potential of the working electrode relative to the reference electrode in the absence of any applied potential or current, and its value reflects the steadiness of the working electrode. Fig. 1(a) shows temperature dependent OCP of arsenopyrite in SAR solution. With time, all the potentials showed slight change to reach a quasi-steady state in about 30 min implying the formation of a spontaneous passivation film to cover the surface of arsenopyrite. All the OCP

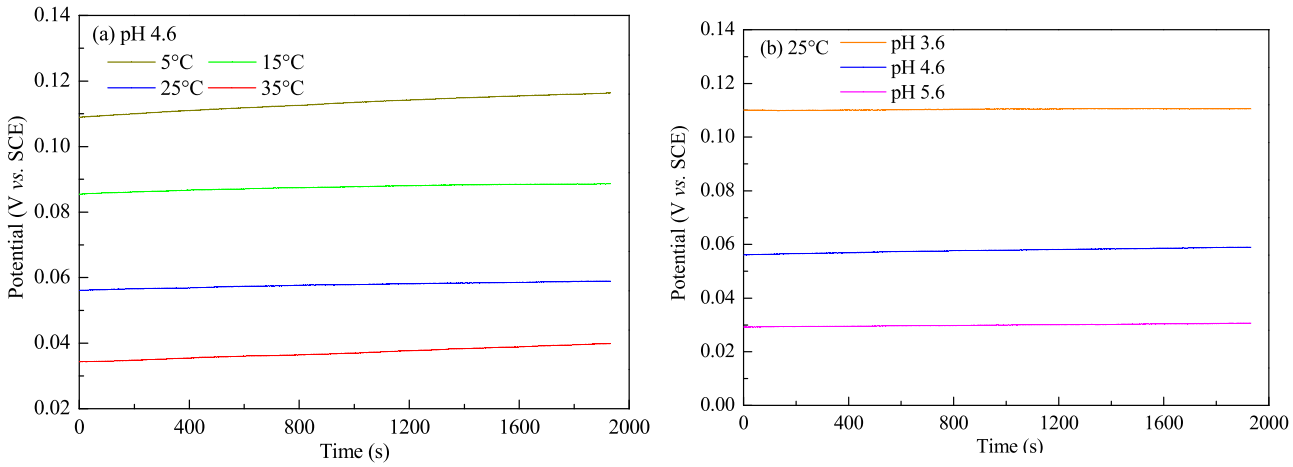

Fig. 1. Variations in the potential with time for the arsenopyrite electrode in simulated acid rain solutions at different temperatures (a) and different pHs (b).

were found to decrease with increasing temperature. Fig. 1(b) shows the OCP values of arsenopyrite in SAR solution having different acidities, with the results indicating increased OCP of arsenopyrite at higher acidities, which was consistent with the report of Moslemi et al. (2011) showing higher mineral electrochemical activity for higher acidity.

As a thermodynamic parameter, the OCP value reflects the weathering trend of arsenopyrite. A more negative OCP value means greater corrosion tendency, i.e., more vulnerability towards erosion, with the reverse being also true. It is worth noting that a higher weathering tendency does not mean a faster weathering rate, for weathering rate is a kinetics parameter, and the weathering rate will discuss at the following polarization measurement. The OCP results (Table 1) showed that both increasing temperature and pH tend to increase the weathering tendency of arsenopyrite and the reason behind may be ineffective formation of passivation film on the electrode surface at higher temperature and the formation of Fe oxyhydroxide coating should be more easily at higher pH (Wang et al., 2018).

3.1.2. Cyclic Voltammetry

Cyclic voltammetry (CV) provides information about the redox reaction and various potential-dependent processes taking place at the interface (Heinze, 1984), hence, was used to study the weathering process of arsenopyrite under various AMD conditions.

Fig. 2 presents the CV diagrams of the weathering of arsenopyrite in SAR solutions at different temperatures and acidities. All the curves had similar redox peaks, indicating similar electrochemical oxidation mechanism of arsenopyrite. Furthermore, temperature and solution pH dependent change of the weathering current suggested that the weathering rate of arsenopyrite was affected by temperature (Corkhill and Vaughan, 2009; Walker et al., 2006; Wang et al., 2021; Yu et al., 2007), as many previous studies have demonstrated. Meanwhile, unbalanced and discrepant anode and cathode currents indicated the irreversible nature of the electrode reactions. When scanned from the OCP to 0.7 V, a faint and narrow anodic peak A1 appeared at approximate 200 mV resulting from the oxidation of arsenopyrite as per reaction (1) (Lazaro et al., 1997). Appearance of another sharply oxidized peak A2 at 600–700 mV was attributed to further oxidation of the substances produced by A1, as per reaction (2)–(4) (Deng and Gu, 2018; Zhang et al., 2020a, 2020b).

Table 1
Open circuit potential of arsenopyrite weathering at different acid rain conditions.

	pH 4.6, different temperatures (°C)				25 °C, different pHs		
	5	15	25	35	5.6	4.6	3.6
OCP (mV)	116	88.5	59.9	39.7	30.2	59.9	110.8

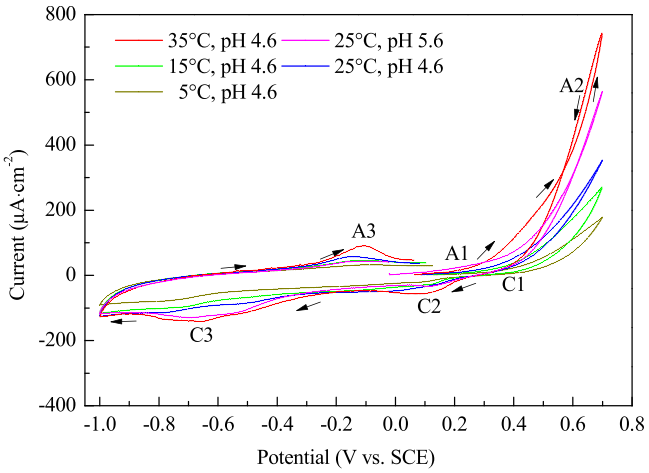

Fig. 2. CV curves for the arsenopyrite electrode in simulated acid rain solutions at different conditions (scan rate 10 mV s^{-1}).

$$A1:\ FeAsS + 3H_2O \rightarrow AsO_3^{3-} + Fe^{2+} + S^0 + 6H^+ + 5e^- \quad (1)$$

$$A2:\ Fe^{2+} \rightarrow Fe^{3+} + e^- \quad (2)$$

$$S^0 + 4H_2O \rightarrow 8H^+ + SO_4^{2-} + 6e^- \quad (3)$$

$$AsO_3^{3-} + H_2O \rightarrow AsO_4^{3-} + 2H^+ + 2e^- \quad (4)$$

When the potential was scanned in the negative direction, three cathodic peaks were detected successively at ~400 mV (C1) (Tu et al., 2017), ~ 150 mV (C2) (Almeida and Giannetti, 2003), and ~650 mV (C3) (Tu et al., 2017), which were due to the reduction of oxides formed in A1 and A2.

$$C1:\ Fe^{3+} + e^- \rightarrow Fe^{2+} \quad (5)$$

$$C2:\ AsO_4^{3-} + 2H^+ + 2e^- \rightarrow AsO_3^{3-} + H_2O \quad (6)$$

$$C3:\ S^0 + 2H^+ + 2e^- \rightarrow H_2S \quad (7)$$

Finally, when the potential was scanned back to OCP, another oxidation peak (A3) appeared at ~− 100 mV, which was attributed to the oxidation of H_2S from reaction C3 (Liu et al., 2011b).

$$A3:\ H_2S \rightarrow S^0 + 2H^+ + 2e^- \quad (8)$$

3.1.3. Polarization

Polarization curve provides information on the arsenopyrite weathering potential (E_{corr}), current density (i_{corr}) and weathering rate (k), and hence can be used to study the thermodynamics and kinetics of the arsenopyrite weathering process. The polarization curves of arsenopyrite in SAR solutions at different temperatures and acidities are shown in Fig. 3. The polarization curves of arsenopyrite display similar *E-i* profiles under varying temperatures or acidities, implying identical electrochemical mechanism and redox reaction of arsenopyrite, which coincided well with the results of above CV. At higher temperature (Fig. 3a), the *E-i* profiles shifted to the lower right along the X- and Y-axis, meaning higher temperature resulted in more negative E_{corr} and greater i_{corr}. Conversely, larger pH value (Fig. 3b) led to the movement of the *E-i* profiles towards the lower left, indicating a more negative E_{corr} and smaller i_{corr} with decreased acidity. Using the Tafel extrapolation theory (Bard and Faulkner, 2001), we can further obtain the weathering rate (k) by extrapolating the values of E_{corr} and i_{corr} by using the Faraday equation:

$$k = \frac{Mi_{corr}}{nF} \tag{9}$$

Where, k (mg cm^{-2} h^{-1}) represents weathering rate, M (g mol^{-1}), n (dimensionless) and F (C mol^{-1}) represent atomic weight, valence state of the element and Faraday constant (96,485 C mol^{-1}), respectively. The detailed polarization parameters obtained are listed in Table 2.

The polarization results showed lower temperature or acidity of acid rain results in more positive corrosion potential, implying more thermodynamics stability of arsenopyrite. Meanwhile, higher temperature or acidity causes higher corrosion rate, namely, faster As(III) releasing rate of arsenopyrite. For example, under different temperature conditions, the value of $k_{(As(III))}$ was 2.80E-4 mg cm^{-2} h^{-1} at 5 °C when the pH was 4.6, implying 24.49 g As(III) at an area of 1 m^2 of FeAsS would be released into the surrounding environment per year. The value was increased to 40.00 g per year when the temperature was increased to 15 °C with 63.2% being the promoting efficiency. As for different acidity conditions, at pH 5.6 the value of $k_{(As(III))}$ was 6.34E-4 mg cm^{-2} h^{-1} which suggested yearly release of 55.50 g As(III) per 1 m^2 area of FeAsS into the surrounding environment, and at pH 4.6 the consequent value was increased to 67.75 g with promoting efficiency of 22.1%.

3.1.4. Electrochemical impedance spectroscopy study

EIS is one of the powerful methods to study the electrochemical process of the electrode/electrolyte interface and widely adopted to study the diffusion and Faraday process of mineral electrodes (Lasia, 2014). The EIS results of arsenopyrite in SAR solutions at different temperatures and acidities are presented in the form of corresponding Nyquist and Bode plots and are displayed in Fig. 4. There were two capacitor loops in all the Nyquist plots at low and high frequency regions and were corresponding to the presence of two time-constants in the Bode plots. The loop at low frequency region was due to the charge transfer resistance associated with the double layer of the electrode/solution interface, while the passive film resistance related to the pseudo-capacitance impedance was responsible for the loop at high frequency. The likely reasons behind the deviations of the loops from ideal semicircle are the variation in the frequency deviation along with the inhomogeneity of the passivation film (Córdoba-Torres et al., 2012). Fig. 4c shows the equivalent electrical circuit (EEC) to simulate the interfacial process between arsenopyrite/solution, where R_s, R_t and R_f represent the solution ohmic resistance, passive film and charge transfers resistance, respectively. As the loops deviated from ideal semicircle, constant phase element CPE_{dl} and CPE_f were used to replace the ideal double layer and passive film capacitance (Córdoba-Torres et al., 2012). Where, the impedance of CPE is $Z_{CPE} = \frac{1}{Y_0(j\omega)^n}$ given by Macdonald (1985), and Z_{CPE} is the impedance of the constant phase element (Ω cm^2), ω is the angular frequency of the AC voltage (rad s^{-1}), Y_0 is the magnitude of admittance of CPE (Ω^{-1} cm^{-2} s^{n}), and n is the exponential term. The values of the different elements in the equivalent circuit are shown in Table 3.

With increasing temperature from 5 °C to 15 °C, the charge transfer resistance R_t for weathering of arsenopyrite decreased from 2.56E5 to 1.72E5, which decreased further to reach 6.63E4 and 3.20E4 at 25 °C and 35 °C, respectively. Meanwhile, increase of temperature from 5 °C to 35 °C with an interval of 10 °C, resulted in the decrease of arsenopyrite weathering passivation film resistance R_f from 5.80E4 to 4.67E4, 2.34E4 and finally to 2.31E4, successively. Along with the decreased resistances, there were corresponding increase of the capacitances of the double layer and passive film. The results showed that higher temperature resulted in a smaller resistance and bigger capacitance at the double layer and passive film, that is, accelerated ions transfer at the double layer and passive film, which were the reasons that higher temperature promoted the weathering of arsenopyrite.

With increasing pH of the solution from 3.6 to 4.6, and finally to 5.6, the R_f for arsenopyrite weathering suffered a decrease from 2.56E4 to 2.34E4, and finally to 1.50E4 Ω cm^2, respectively, while there was increase of the CPE_f from 2.41E-5–5.13E-5, and to 8.82E-5 Ω cm^2. Meanwhile, R_t rose from 2.61E4 to 6.63E4, and to 7.15E4 Ω cm^2, with the CPE_f dropping from 1.57E-3 to 5.44E-4, and to 1.39E-4 Ω cm^2, indicating the decrease of R_t and increase of R_f increasing acidity. A smaller value of R_t suggests charge easily transfer at the double layer, meaning higher acidity promotes arsenopyrite weathering; Meanwhile, larger value of R_f suggests thicker passivation film, meaning higher acidity inhibits arsenopyrite weathering. Comparing the values of R_t and

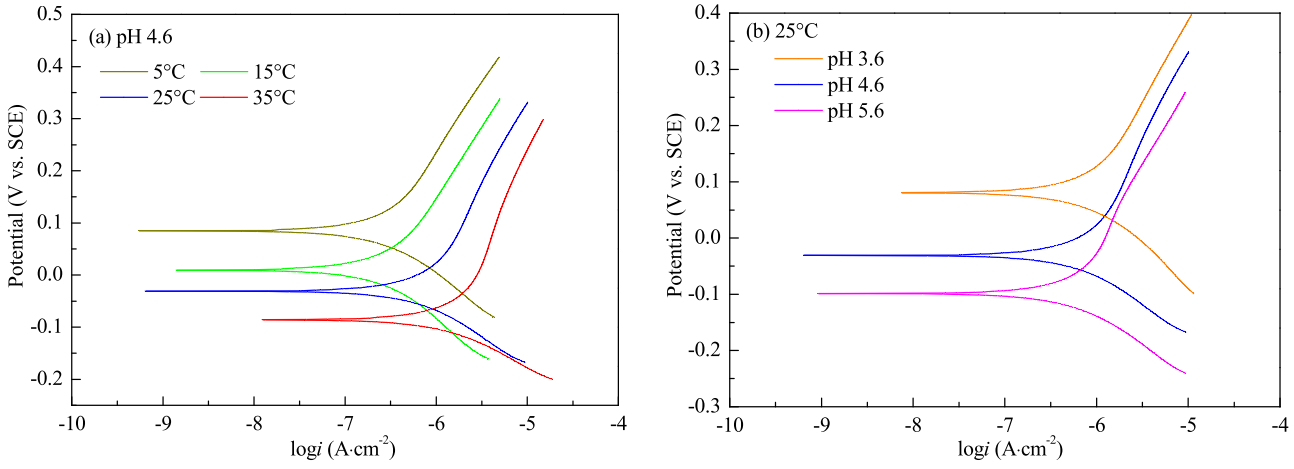

Fig. 3. Polarization curves of arsenopyrite in simulated acid rain solutions at different temperatures (a) and different pHs (b).

Table 2
Tafel parameters of arsenopyrite weathering at different acid rain conditions.

	pH	Temperature (°C)	E_{corr} (mV)	i_{corr} (μA cm^{-2})	$k_{(As(III))}$ (mg cm^{-2} h^{-1})
Different temperatures	4.64.64.6	5	86.2	0.30	2.80E-4
		15	10.8	0.49	4.57E-4
		25	-30.0	0.83	7.73E-4
		35	-84.4	1.11	1.03E-3
Different pHs	5.6	25	-98.7	0.68	6.34E-4
	4.6	25	-30.0	0.83	7.73E-4
	3.6	25	80.7	1.20	1.12E-3

E_{corr}: corrosion potential; i_{corr}: corrosion current density; k: corrosion rate.

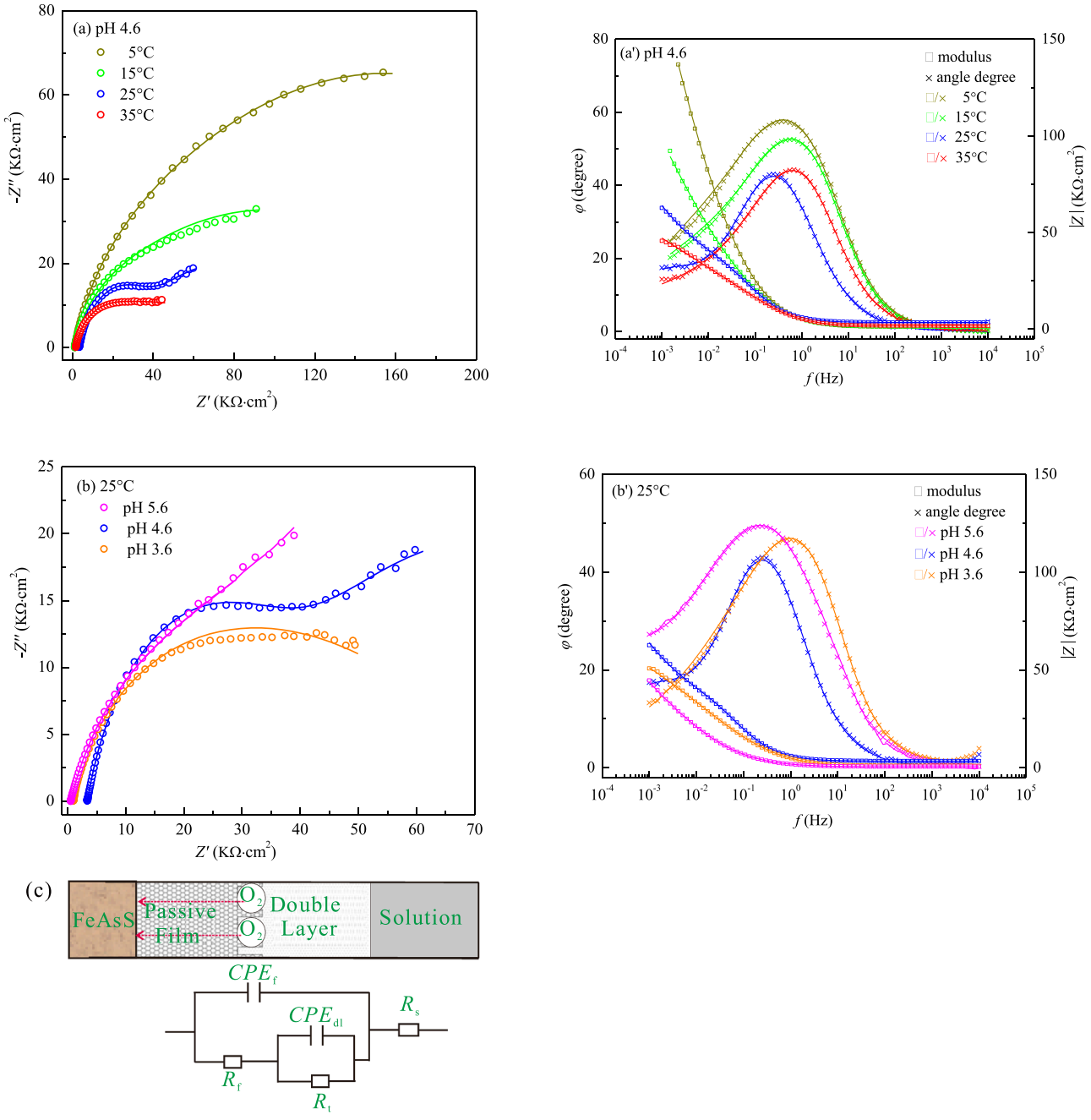

Fig. 4. Nyquist (a, b) and Bode plots (a′, b′) and equivalent circuits (c) for arsenopyrite in simulated acid rain solutions at different temperatures and different pHs, where ○, □ and × represent the experimental values and — represents simulated values.

Table 3
Equivalent circuit model parameters of arsenopyrite weathering at different acid rain conditions.

	pH	Temperature (°C)	CPE_f, Y_0 (S cm^{-2} s^{-n})	n	R_f (Ω cm^2)	CPE_{dl}, Y_0 (S cm^{-2} s^{-n})	n	R_t (Ω cm^2)	χ^2
Different temperatures	4.6	5	4.70E-5	0.800	5.80E4	4.86E-5	0.480	2.56E5	3.55E-4
	4.6	15	4.93E-5	0.771	4.67E4	2.96E-4	0.668	1.72E5	8.47E-4
	4.6	25	5.13E-5	0.769	2.34E4	5.44E-4	0.607	6.63E4	1.54E-4
	4.6	35	5.35E-5	0.773	2.31E4	7.86E-4	0.541	3.20E4	6.41E-5
Different pHs	5.6	25	8.82E-5	0.806	1.50E4	1.39E-4	0.732	7.15E4	1.20E-4
	4.6	25	5.13E-5	0.769	2.34E4	5.44E-4	0.607	6.63E4	1.54E-4
	3.6	25	2.41E-5	0.745	2.56E4	1.57E-3	0.905	2.61E4	3.24E-3

R_f: passive film resistance; R_t: charge transfer resistance; n: dimensionless number; CPE_{dl}: constant phase element of double layer; CPE_f: constant phase element of passive film

R_f at a same acidity, the value of R_t is always greater than that of R_f, suggesting that R_t is the controlling factor of the arsenopyrite weathering, that is, higher acidity promotes arsenopyrite weathering though produce more passivation film. The reason is when increases the concentration of H^+ ions, it is advantage of O_2 reduced to H_2O (Reaction (10)), and thus promotes ansenopyrite weathering in turn and produce more S^0 and As(III) (Reaction (1)).

$$O_2 + 4H^+ + 4e^- \rightarrow H_2O \quad (10)$$

3.2. Arsenopyrite weathering activation thermodynamic parameters

Activation energy (E_a) refers to the energy required for a molecule to transform from a normal state to an excited state from where the chemical reactions easily occur. Generally, smaller activation energy implies easy transformation of the molecule into the activated state which suggests more likely occurrence of the weathering reaction. Activation enthalpy (ΔH^*) is an important thermodynamic parameter representing the energy absorbed or released by the system. When $\Delta H^* > 0$, the process is endothermic implying increase of weathering rate with increasing temperature. When $\Delta H^* < 0$, the process is an exothermic one. The essence of entropy (ΔS^*) is the "inner chaos" of a system; $\Delta S^* > 0$ representing the entropy increase indicating that the molecule is progressing from the ground state to the activated state, i.e., is a process from order to disorder; $\Delta S^* < 0$ represents the process of reducing chaos. (Atkins, 2002).

Arrhenius equation (Arrhenius, 1889) established the relationship between reaction rate and temperature, and can be used for calculate the activation energy.

$$\ln k = -\frac{E_a}{RT} + \ln A \quad (11)$$

Here: k is the corrosion rate, mg cm^{-2} h^{-1}; E_a is the activation energy, kJ mol^{-1}; R is the universal gas constant, 8.314 J mol^{-1} K^{-1}; T is the absolute temperature, K; and A is a pre-exponential factor. Based on the above polarization results (Table 2), the relationship between ln$k$ and $1/T$ for arsenopyrite in SAR is shown in Fig. 5(a), and the obtained relationship was $\ln k = -3824.8/T + 10.305$, $R^2 = 0.9914$. From the relationship, the activation energy for the weathering of arsenopyrite was obtained to be 31.80 kJ mol^{-1}. Badawy et al. (2000) pointed out ready interaction for activation energy less than 40 kJ mol^{-1} and thus the obtained activation energy suggested easy weathering of arsenopyrite in SAR. Furthermore, the value of $E_a > 20$ kJ mol^{-1} further confirmed that the oxidative dissolution of arsenopyrite was controlled by the surface reaction control from the view of dissolution kinetics (Lasaga, 1998).

According to the transition state theory, the activation enthalpy (ΔH^*) and activation entropy (ΔS^*) of arsenopyrite weathering, can be calculated from Eq. (12) (Hegazy et al., 2012):

$$ln\left(\frac{k}{T}\right) = \left(ln\left(\frac{R}{N_A h}\right) + \left(\frac{\Delta S^*}{R}\right)\right) - \frac{\Delta H^*}{RT} \quad (12)$$

where, k is the corrosion rate, mg cm^{-2} h^{-1}; T is the absolute temperature, K; N_A is Avogadro's number, 6.02E23 mol^{-1}; h is the Planck's constant, 6.626E-34 J s; R is the universal gas constant, 8.314 J mol^{-1} K^{-1}. In this work, the linear relationship between ln(k/T) and 1/T was ln(k/T) = $-3532.21/T + 3.6253$ ($R^2 = 0.9897$) (Fig. 5b), from which the obtained values of ΔH^* and ΔS^* for the weathering of arsenopyrite were 29.37 kJ mol^{-1} and − 167.40 J mol^{-1} K^{-1}, respectively. The value of $\Delta H^* > 0$ indicating the endothermic nature of the weathering process of arsenopyrite and reflected heating is conducive to the weathering of arsenopyrite (Refaey et al., 2004), corresponding to the previous electrochemical results. $\Delta S^* < 0$ suggested that the activated process was associated rather than dissociated in the rate-determining-step, that is, the disorder has been reduced from the reactant to transition state/-activated complex (Benabdellah et al., 2006).

3.3. Characterizations

3.3.1. Mineral chemical structural analysis

Raman spectroscopic analysis provides the chemical structural information of the mineral and identifies the characteristic peaks of the original and eroded arsenopyrite (Neil et al., 2014). The Raman spectra of arsenopyrite in SAR solutions at different temperatures and acidities

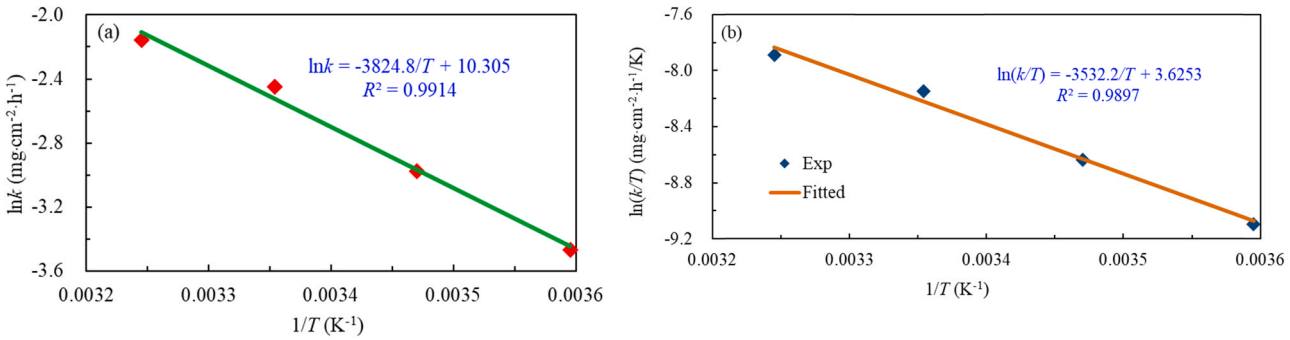

Fig. 5. The relationship between ln$k$ versus $1/T$ (a) and lnk/T versus $1/T$ (b) for arsenopyrite in simulated acid rain solutions.

are presented in Fig. S2. For the pristine arsenopyrite, five Raman peaks are observed at 135, 171, 274, 334, and 404 cm^{-1}, respectively, and are consistent with the characteristic peaks of arsenopyrite (Filippi et al., 2015; McGuire et al., 2001a). After being weathered for two months, appearance of four additional peaks at 151, 217, 471 and 845 cm^{-1} was observed in the arsenopyrite sample. The peaks appearing at 151, 217, and 471 cm^{-1} were attributed to the elemental sulfur (S^0) (Murciego et al., 2019; Xia et al., 2010), while the peak occurring at 845 cm^{-1} was ascribed to arsenate (AsO_4^{3-}) (v_3, asymmetric stretching mode) as from the previous literature reports (Filippi et al., 2015; Frost et al., 2012). The Raman spectroscopy confirmed the products S^0 and AsO_4^{3-}. AsO_4^{3-} and Fe^{3+} easily combine to precipitate $FeAsO_4$ (scorodite) for its low solubility ($\log Ksp(FeAsO_4) = 5.7 \times 10^{-21}$ (Dean, 1999)). The production of $FeAsO_4$ and S^0 are adhered on the arsenopyrite surface, acting as a passivation film and inhibit the arsenopyrite weathering, which is in confirmation with the previous study (Corkhill and Vaughan, 2009). According to Fernandez et al. (1996a) oxidation of arsenopyrite can only take place when the ions diffuse through the surface passivation layer. McGuire et al. (2001b) observed that formation of passivation film in patches rather than a 'blanket-overlayer' allowed oxidation to continue on the surface. According to Mikhlin et al. (2006) decomposition of the passivation layer under high over-potential accelerates the progress of oxidation, corresponding to the promotion of the weathering of arsenopyrite by higher temperature and acidity. The Raman peak positions of FeAsS, S^0 and AsO_4^{3-} are summarized in Table S2.

3.3.2. *Surface elemental composition analysis*

XPS provides the chemical state of mineral surface elements (Mikhlin et al., 2006), and hence was used to investigate the change of chemical state and contents (at%) of the elements As, S, and Fe in arsenopyrite before and after being weathered in SAR.

Fig. 6 displayed the As $3d_{(5/2)}$ spectra for the pristine and eroded arsenopyrite. For the pristine arsenopyrite specimen, there were three double peaks appearing at approximately 41.6, 43.6 and 44.9 eV, corresponding to As(-I)-S (70.2%), As(I)-O (13.1%) and As(III)-O (16.7%), respectively, and thus mainly existing as As(-I)-O. The eroded arsenic species displayed four double peaks at approximately 41.6, 43.6, 44.9 and 45.7 eV, which were attributed to As(-I)-O, As(I)-O, As(III)-O and As (V)-O, respectively (Corkhill et al., 2008; Mikhlin et al., 2006), and thus mainly existing as As(III)-O and As(V)-O. This reveal the oxidation of As in FeAsS through double-electron transfer steps during the weathering process, as per the transform sequence (13). Moreover, gradual increase of temperature from 5 °C to 35 °C at the pH 4.6 led to the increase of As (V)-O content from 29.0% to 42.8%. As(V)-O also increased from 30.0% to 42.9%, when the pH was reduced from 5.6 to 3.6 leading to increased acidity (Table S3). The results imply that increasing temperature or acidity promote the oxidation of arsenic species.

$$As^{-} \rightarrow As^{+} \rightarrow As^{3+} \rightarrow As^{5+} \quad (13)$$

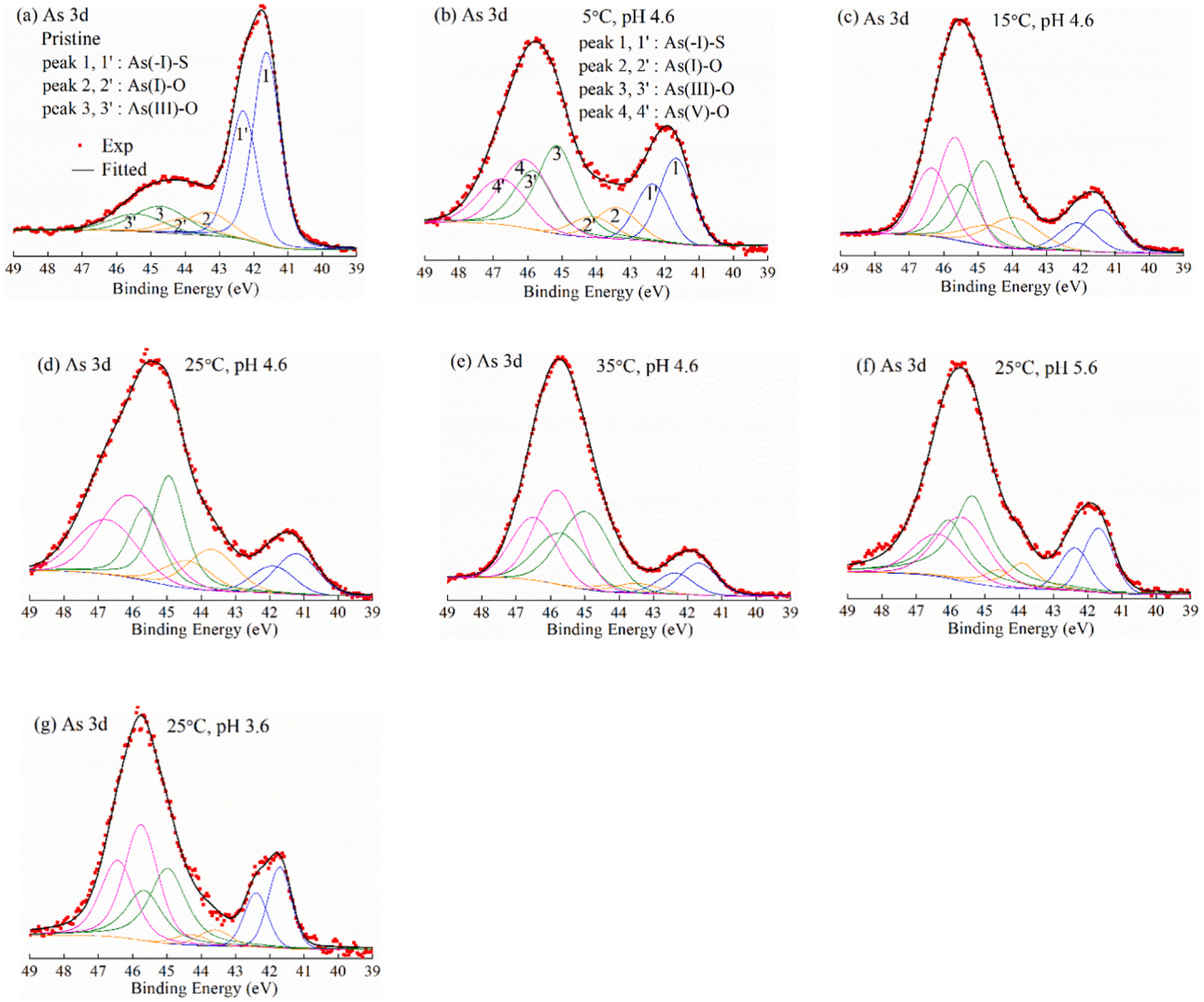

Fig. 6. XPS spectra for As 3d (a-g) in the pristine and eroded surfaces of arsenopyrite.

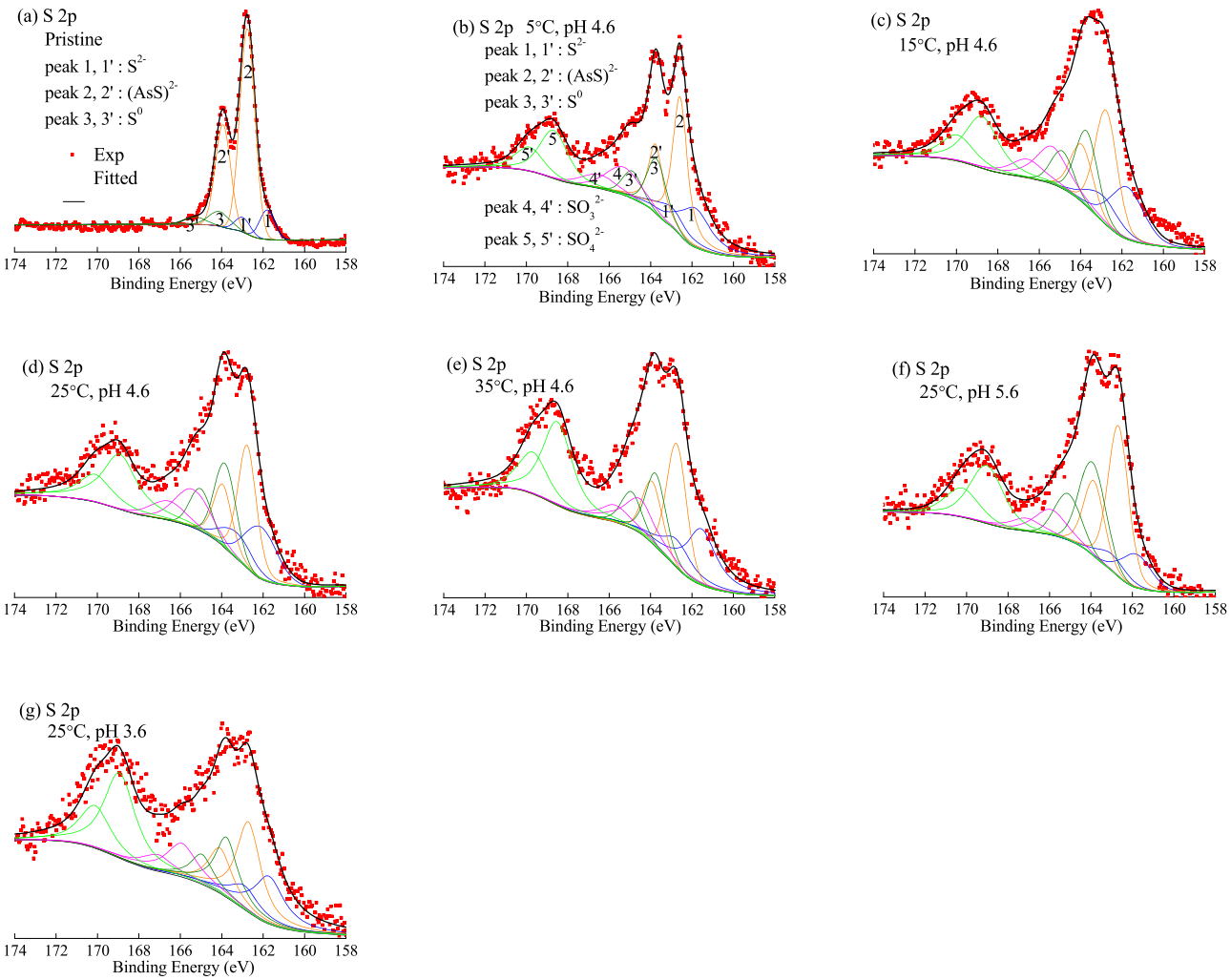

Fig. 7. XPS spectra for S 2p(a-g) in the pristine and eroded surfaces of arsenopyrite.

Fig. 7 display the S $2p_{(3/2)}$ spectra of the pristine and eroded arsenopyrite. There are five double peaks at 161.7, 162.7, 163.9, 166 and 168.6 eV, and can be ascribed to S^{2-}, $(AsS)^{2-}$, S^0, SO_3^{2-} and SO_4^{2-}, respectively (Nesbitt et al., 1995; Zhang et al., 2020a, 2020b). The pristine sample mainly contains sulfur as S^{2-} (11.5%), $(AsS)^{2-}$ (80.5%) and S^0 (8.0%), with $(AsS)^{2-}$ being the major component, while the eroded samples show two additional SO_3^{2-} and SO_4^{2-} components in comparison to the pristine sample. With increasing temperature and acidity, there is gradual increase in the content of SO_4^{2-} with simultaneous decrease of the content of $(AsS)^{2-}$ (Table S4). The results revealed that the S component of FeAsS was gradually oxidized to S^0, SO_3^{2-} and finally transforming to SO_4^{2-} during the weathering process.

Fig. 8 display the Fe $2p_{(3/2)}$ spectra of pristine and eroded arsenopyrite. The pristine iron species consisted of Fe(II)-AsS (706.7, 707.5 and 708.5 eV), Fe(III)-AsS (709.1, 710.1, 711.1 and 712.1 eV) and a small fraction of Fe(III)-O (711.3, 712.3, 713.3 and 714.3 eV) according to GS multiplets (Corkhill et al., 2008; Liu et al., 2020), while Fe(II)-AsS is the major ingredient accounting for 56.65%. The eroded iron species contained extra peaks at 714.6, 715.6 and 716.6 eV, and can be assigned to Fe(III)-SO formed by the oxidation of arsenopyrite with its content increasing with temperature and acidity (Table S5). The results indicate that higher temperature or acidity accelerates the conversion of ferrous (Fe^{2+}) to ferric (Fe^{3+}), for higher temperature or lower pH advantage of the reduce of oxygen (Reaction (10)) and promotes the oxidized of Fe^{2+} in turn (Reaction (2)). Furthermore, the generated Fe^{3+} as an oxidant will further promote the weathering of arsenopyrite, as per reaction (14) (Yu et al., 2007).

$$FeAsS + 7H_2O + 11Fe^{3+} \rightarrow AsO_3^{3-} + 12Fe^{2+} + SO_4^{2-} + 14H^+ \quad (14)$$

In summary, the chemical states of all the elements in pristine arsenopyrite mainly correspond to low valence having lower binding energy, whereas the eroded arsenopyrite mainly correspond to high oxidation-state components related to higher binding energy regions. The content of high-valence elements showed increasing trend with the increase of temperature and acidity and reached over 83.3% (AsO_3^{3-} and AsO_4^{3-}), 56.4% (S^0, SO_3^{2-} and SO_4^{2-}) and 89.5% (Fe^{3+}) at pH 4.6 and 35 °C. All these results confirmed that higher temperature or acidity was favorable for the weathering of arsenopyrite.

3.4. Summarization of the weathering mechanism of Arsenopyrite

The weathering mechanism of arsenopyrite in acid rain is summarized in Fig. 9 based on the combined results from the electrochemical measurements and surface analysis. Arsenopyrite weathering is an electrochemical oxidation process, which is consisting of three steps: anodic oxidation, electron transfer and cathode reduction. In anodic oxidation, FeAsS is firstly oxidized to low-valence Fe^{2+}, AsO_3^{3-} and S^0, followed by the release of H^+ ions, causing AMD pollution. Fe^{2+} is gradually converted to high-valence Fe^{3+}. S^0 is transformed to the intermediate product SO_3^{2-} and ultimately to SO_4^{2-}, meanwhile, AsO_3^{3-} was oxidized to AsO_4^{3-}. $Fe^{3+}$and AsO_4^{3-} may further combine to form $FeAsO_4$ because of its very low solubility. The $FeAsO_4$ and S^0 can easily adsorbed

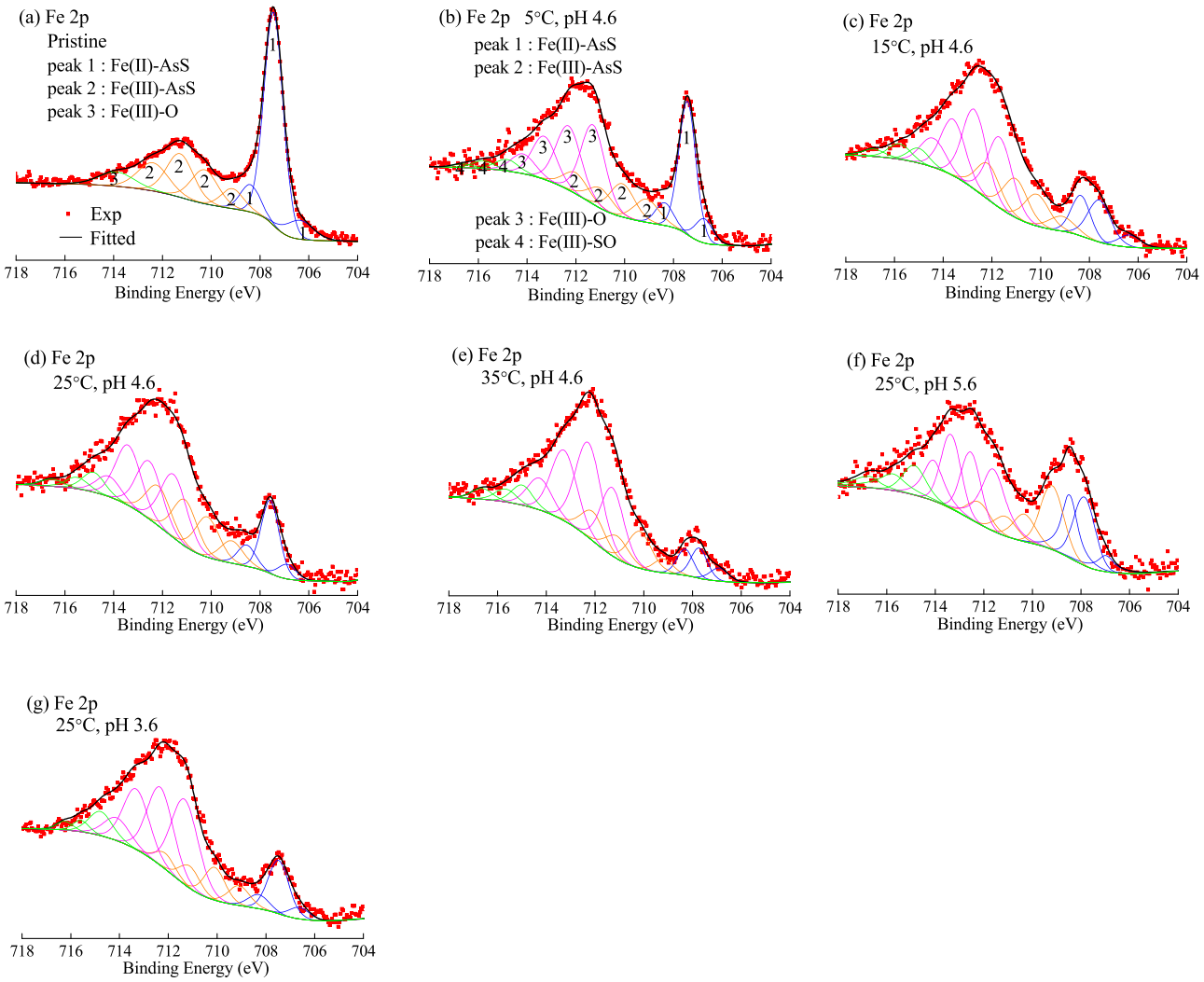

Fig. 8. XPS spectra for Fe 2p (a–g) in the pristine and eroded surfaces of arsenopyrite.

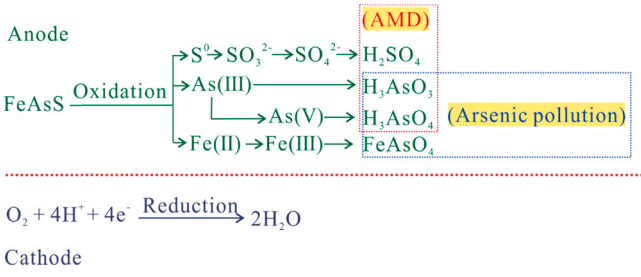

Fig. 9. Scheme of the weathering mechanism of arsenopyrite in simulated acid rain solutions.

on the surface of arsenopyrite and inhibit the weathering of arsenopyrite. In the cathode, dissolved oxygen is reduced.

4. Environmental implications

During erosion of arsenopyrite in acid rain, release of arsenic and H^+ ions takes place leading to the pollution of surrounding environment. Environmental temperature and the acidity of acid rain have great effect on the weathering process. Higher temperature or higher acidity will increase the weathering tendency of arsenopyrite according to the results of open current potential and corrosion potential measurements. The accumulations of arsenopyrite weathering products like Fe^{3+} and H^+ will cause further deterioration of the surrounding environment. In the mine area, when governments are concerned with acid rain control, attention should also be put to arsenopyrite mineral and arsenopyrite tailings' exploitation and transportation at the mining area, to avoid arsenopyrite weathering in acid rain resulting in serious environmental issues.

5. Conclusions

Electrochemical techniques and surface analysis techniques were used to study the weathering behaviors of arsenopyrite in simulated acid rain solution. At the initial stage, oxidation of FeAsS to Fe^{2+}, AsO_3^{3-} and S^0 takes place, followed by the conversion of Fe^{2+} to Fe^{3+}, S^0 to SO_3^{2-} and ultimately to SO_4^{2-}, and AsO_3^{3-} to AsO_4^{3-}. Higher temperature or acidity of AMD increased the weathering trend of arsenopyrite, and also accelerated the arsenopyrite weathering rate causing smaller resistance and greater capacitance at the double layer and passivation film, with the rate constant approximately being 10^{-8} mol m^{-2} s^{-1}. The relationship between the arsenopyrite weathering rate and temperature was $\ln k = -3824.8/T + 10.305$, with the thermodynamic parameters of ΔH^* and ΔS^* found to be 29.37 kJ mol^{-1} and − 167.40 J mol^{-1} K^{-1}, respectively. This study provides a theoretical basis for rapid and quantitative assessment of arsenopyrite pollution by means of in-situ electrochemical technology. We also showed the significance in

assessing the risks of arsenopyrite in the acid rain area towards the surrounding area.

CRediT authorship contribution statement

Xiaonan Feng and **Qingyou Liu** designed research; **Xiaonan Feng**, **Qingyou Liu, Shuai Wang**, **Ling Cen** and **Heping Li** performed research; **Xiaonan Feng**, **Shuai Wang** and **Qingyou Liu** analyzed data; **Xiaonan Feng** and **Qingyou Liu** wrote the paper; **Qingyou Liu** and **Heping Li** gave Funding acquisition, Project administration.

The authors declare no competing interest.

Declaration of Competing Interest

The authors declare that they have no known competing financial interests or personal relationships that could have appeared to influence the work reported in this paper.

Acknowledgments

This work was financially supported by project of National Natural Science Foundation of China (U1812402), the National Natural Science Foundation of China (41873074), and the Strategic Priority Research Program (XDB 18010401), CAS.

Appendix A. Supporting information

Supplementary data associated with this article can be found in the online version at doi:10.1016/j.jhazmat.2021.126612.

References

Almeida, C.M., Giannetti, B.F., 2003. Electrochemical study of arsenopyrite weathering. Phys. Chem. Chem. Phys. 5 (3), 604–610.
An, C.H., 2015. Acid rain and its control in Dongchuan. Environ. Sci. Surf. 34 (1), 45–49 (In Chinese with English abstract).
Arrhenius, S., 1889. On the reaction velocity of the inversion of cane sugar by acids. Z. Phys. Chem. 4, 226–248.
Atkins, P., 2002. Atkins' Physical Chemistry. Oxford University Press, Oxford, Britain.
Badawy, W.A., Al-Kharafi, F.M., Al-Ajmi, J.R., 2000. Electrochemical behaviour of cobalt in aqueous solutions of different pH. J. Appl. Electrochem. 30 (6), 693–704.
Bard, A.J., Faulkner, L.R., 2001. Electrochemical Methods: Fundamentals and Applications, 2nd ed. Wiley and Sons, Hoboken.
Benabdellah, M., Aouniti, A., Dafali, A., Hammouti, B., Benkaddour, M., Yahyi, A., 2006. Investigation of the inhibitive effect of triphenyltin 2-thiophene carboxylate on corrosion of steel in 2 M H_3PO_4 solutions. Appl. Surf. Sci. 252, 8341–8347.
Córdoba-Torres, P., Mesquita, T., Devos, O., Tribollet, B., Roche, V., Nogueira, R., 2012. On the intrinsic coupling between constant-phase element parameters a and Q in electrochemical impedance spectroscopy. Electrochim. Acta 72, 172–178.
Corkhill, C.L., Vaughan, D.J., 2009. Arsenopyrite oxidation-a review. Appl. Geochem. 24, 2342–2361.
Corkhill, C.L., Wincott, P.L., Lloyd, J.R., Vaughan, D.J., 2008. The oxidative dissolution of arsenopyrite (FeAsS) and enargite (Cu_3AsS_4) by Leptospirillum ferrooxidans. Geochim. Cosmochim. Acta 72, 5616–5633.
Coussy, S., Benzaazoua, M., Blanc, D., Moszkowicz, P., Bussière, B., 2011. Arsenic stability in arsenopyrite-rich cemented paste backfills: a leaching test-based assessment. J. Hazard. Mater. 185, 1467–1476.
Cui, J., Zhou, J., Peng, Y., He, Y., Yang, H., Mao, J., 2014a. Atmospheric wet deposition of nitrogen and sulfur to a typical red soil agroecosystem in Southeast China during the ten-year monsoon seasons (2003–2012). Atmos. Environ. 82, 121–129.
Cui, J., Zhou, J., Peng, Y., He, Y., Yang, H., Mao, J., Zhang, M., Wang, Y., Wang, S., 2014b. Atmospheric wet deposition of nitrogen and sulfur in the agroecosystem in developing and developed areas of Southeastern China. Atmos. Environ. 89, 102–108.
Dean, J.A., 1999. Lange's Handbook of Chemistry, Fifteenth ed. Mcgraw-Hill, Inc, St. Lous.
Deng, S., Gu, G., 2018. An electrochemical impedance spectroscopy study of arsenopyrite oxidation in the presence of Sulfobacillus thermosulfidooxidans. Electrochim. Acta 287, 106–114.
Deng, S., Gu, G., He, G., Li, L., 2018. Catalytic effect of pyrite on the leaching of arsenopyrite in sulfuric acid and acid culture medium. Electrochim. Acta 263, 8–16.
Fernandez, P.G., Linge, H.G., Wadsley, M.W., 1996a. Oxidation of arsenopyrite (FeAsS) in acid part I: reactivity of arsenopyrite. J. Appl. Electrochem. 26, 575–583.
Filippi, M., Drahota, P., Machovič, V., Böhmová, V., Mihaljevič, M., 2015. Arsenic mineralogy and mobility in the arsenic-rich historical mine waste dump. Sci. Total Environ. 536, 713–728.
Frost, R.L., Xi, Y.F., Tan, K.Q., Millar, G.J., Palmer, S.J., 2012. Vibrational spectroscopic study of the mineral pitticite Fe, AsO_4, SO_4, H_2O. Spectrochim. Acta A 85, 173–178.
Glodowska, M., Stopelli, E., Schneider, M., Lightfoot, A., Rathi, B., Straub, D., Patzner, M., Duyen, V.T., AdvectAs Team, M., Berg, M., Kleindienst, S., Kappler, A., 2020. Role of in situ natural organic matter in mobilizing As during microbial reduction of Fe(III)-mineral-bearing aquifer sediments from Hanoi (Vietnam). Environ. Sci. Technol. 54 (7), 4149–4159.
Gupta, R.P., Sen, S.K., 1974. Calculation of multiplet structure of core p-vacancy levels. Phys. Rev. B 10, 71–79.
Gupta, R.P., Sen, S.K., 1975. Calculation of multiplet structure of core p-vacancy levels II. Phys. Rev. B 12, 15–19.
Hammond, C.M., Root, R.A., Maier, R.M., Chorover, J., 2020. Arsenic and iron speciation and mobilization during phytostabilization of pyritic mine tailings. Geochim. Cosmochim. Acta 286, 306–323.
Hegazy, M.A., El-Tabei, A.S., Bedair, A.H., Sadeq, M.A., 2012. An investigation of three novel nonionic surfactants as corrosion inhibitor for carbon steel in 0.5 M H_2SO_4. Corros. Sci. 54, 219–230.
Heinze, J., 1984. Cyclic voltammetry - "electrochemical spectroscopy". New analytical methods (25). Angew. Chem. Int. Ed. Engl. 23, 831–847.
Hiskey, J.B., Sanchez, V., 1987. Electrochemical oxidation of arsenopyrite in alkaline media. JOM J. Min. Met. Mat. Soc. 39 (10), A1.
Kostina, G.M., Chernyak, A.S., 1979a. Kenetics of electrochemical oxidation of arsenopyrite and pyrite in caustic soda solutions. J. Appl. Chem. 52 (4), 732.
Kostina, G.M., Chernyak, A.S., 1979b. Investigation of the mechanism of electrochemical Oxidation of arsenopyrite and pyrite in caustic soda solutions. J. Appl. Chem. 52 (7), 1457.
Larssen, T., Schnoor, J.L., Seip, H.M., Dawei, Z., 2000. Evaluation of different approaches for modeling effects of acid rain on soils in China. Sci. Total Environ. 246 (2–3), 175–193.
Lasaga, A., 1998. Kinetic Theory in the Earth Sciences. Princeton series in geochemistry. Princeton university press, Princeton, New Jersey.
Lasia, A., 2014. Electrochemical Impedance Spectroscopy and its Applications. Springer, New York, pp. 2–3.
Lazaro, I., Cruz, R., Gonzalez, I., Monroy, M., 1997. Electrochemical oxidation of arsenopyrite in acidic media. Int. J. Miner. Process. 50 (1–2), 63–75.
Li, T., Wang, X., Zhou, Q.X., Liao, C.M., Zhou, L., Wan, L.L., An, J.K., Du, Q., Li, N., Ren, Z.Z., 2018. Swift acid rain sensing by synergistic rhizospheric bioelectrochemical responses. ACS Sens. 3, 1424–1430.
Lin, H.K., Zheng, Z.M., 1996. Electrochemical oxidation of arsenopyrite in chloride solutions. Hydrometallurgy 42 (3), 411–424.
Liu, X.L., Li, Q., Zhang, Y., Jiang, T., Yang, Y.B., Xu, B., He, Y.H., 2020. Electrochemical behaviour of the dissolution and passivation of arsenopyrite in 9K culture medium. Appl. Surf. Sci. 508, 145269.
Liu, Y., Dang, Z., Wu, P., Lu, J., Shu, X., Zheng, L., 2011b. Influence of ferric iron on the electrochemical behavior of pyrite. Ionics 17, 169–176.
Lizaro, I., Cruz, R., Gonzilez, I., Monroy, M., 1997. Electrochemical oxidation of arsenopyrite in acidic Media. Int. J. Miner. Process. 50, 63–75.
Macdonald, J.R., 1985. Generalizations of "'universal dielectric response"' and a general distribution-of-activation-energies model for dielectric and conducting systems. J. Appl. Phys. 58, 1971–1978.
McGuire, M.M., Jallad, K.N., Ben-Amotz, D., Hamers, R.J., 2001a. Chemical mapping of elemental sulfur on pyrite and arsenopyrite surfaces using near-infrared Raman imaging microscopy. Appl. Surf. Sci. 178, 105–115.
McGuire, M.M., Edwards, K.J., Banfield, J.F., Hamers, R.J., 2001b. Kinetics, surface chemistry, and structural evolution of microbially mediated sulfide mineral dissolution. Geochim. Cosmochim. Acta 65, 1243–1258.
Mikhlin, Y.L., Romanchenko, A.S., Asanov, I.P., 2006. Oxidation of arsenopyrite and deposition of gold on the oxidised surfaces: a scanning probe microscopy, tunneling spectroscopy and XPS study. Geochim. Cosmochim. Acta 70, 4874–4888.
Moldovan, C., Sbirna, S., Ionescu, C., Sbirna, L.S., Codresi, C., 2014. Simulated impact of acid rain on organic matter, phosphorus and other soil components. Environ. Eng. Manag. J. 13 (6), 1389–1392.
Moslemi, H., Shamsi, P., Habashi, F., 2011. Pyrite and pyrrhotite open circuit potentials study: effects on flotation. Miner. Eng. 24 (10), 1038–1045.
MuñOz, J.A., Gómez, C., Ballester, A., Blažquez, M.L., Gonzalez, F., Figueroa, M., 1998. Electrochemical behaviour of chalcopyrite in the presence of silver and Sulfolobus bacteria. J. Appl. Electrochem. 28 (1), 49–56.
Murciego, A., Álvarez-Ayuso, E., Aldana-Martínez, S.C., Sanz-Arranz, A., Medina-García, J., Rull-Pérez, F., Villar-Alonso, P., 2019. Characterization of secondary products in arsenopyrite-bearing mine wastes: influence of cementation on arsenic attenuation. J. Hazard. Mater. 373, 425–436.
Neil, C.W., Yang, Y., Schupp, J., Jun, Y, D., 2014. Water chemistry impacts on arsenic mobilization from arsenopyrite dissolution and secondary mineral precipitation: implications for managed aquifer recharge. Environ. Sci. Technol. 48, 4395–4405.
Nesbitt, H.W., Muir, I.J., Pratt, A.R., 1995. Oxidation of arsenopyrite by air and airsaturated, distilled water and implications for mechanisms of oxidation. Geochim. Cosmochim. Acta 59, 1773–1786.
Nordstrom, D.K., 2009. Acid rock drainage and climate change. J. Geochem. Explor. 100 (2–3), 97–104.
Refaey, S.A.M., Taha, F., Abd El-Malak, A.M., 2004. Inhibition of stainless steel pitting corrosion in acidic medium by 2-mercaptobenzoxazole. Appl. Surf. Sci. 236, 175–185.
Sanchez, V., Hiskey, J.B., 1988. An electrochemical study of the surface oxidation of arsenopyrite in alkaline media. MTB B 19 (6), 943–949.
Silva, R.A., Park, J., Ilyas, S., Borja, D., Zhao, H., Urík, M., Rastegar, S.O., Kim, H., 2020. Biodegradation mechanism of arsenopyrite mine tailing with Acidithiobacillus

ferrooxidans and influence of ferric supplements. Int. Biodeterior. Biodegrad. 153, 108522.
Tu, Z., Wan, J., Guo, C., Fan, C., Zhang, T., Lu, G., Reinfelder, J.R., Dang, Z., 2017. Electrochemical oxidation of pyrite in pH 2 electrolyte. Electrochim. Acta 239, 25–35.
Walker, F.P., Schreiber, M.E., Rimstidt, J.D., 2006. Kinetics of arsenopyrite oxidative dissolution by oxygen. Geochim. Cosmochim. Acta 70, 1668–1676.
Wang, S., Jiao, B., Zhang, M., Zhang, G., Wang, X., Jia, Y., 2018. Arsenic release and speciation during the oxidative dissolution of arsenopyrite by O_2 in the absence and presence of EDTA. J. Hazard. Mater. 346, 184–190.
Wang, S., Zheng, K., Li, H.P., Feng, X.N., Wang, L.Y., Liu, Q.Y., 2021. Arsenopyrite weathering in acidic water: humic acid affection and arsenic transformation. Water Res. 194, 116917.
Wang, X., Chen, L., Yoshimura, N., 2000. Erosion by acid rain, accelerating the tracking of polystyrene insulating material. J. Phys. D Appl. Phys. 33, 1117–1127.
Xia, J.L., Yang, Y., He, H., 2010. Surface analysis of sulfur speciation on pyrite bioleached by extreme thermophile Acidianus manzaensis using Raman and XANES spectroscopy. Hydrometallurgy 100, 129–135.
Yu, Y., Zhu, Y., Gao, Z., Gammons, C.H., Li, D., 2007. Rates of arsenopyrite oxidation by oxygen and Fe(III) at pH 1.8–12.6 and 15–45 °C. Environ. Sci. Technol. 41, 6460–6464.
Zeman, K., Mandl, M., Mrnustikova, P., 1995. Oxidation of arsenopyrite by Thiobacillus-Ferrooxidans detected by a mineral electrode. Biotechnol. Tech. 9 (2), 111–116.
Zhang, D.R., Chen, H.R., Xia, J.L., Nie, Z.Y., Fan, X.L., Liu, H.C., Zheng, L., Zhang, L.J., Yang, H.Y., 2020a. Humic acid promotes arsenopyrite bio-oxidation and arsenic immobilization. J. Hazard. Mater. 384, 121359.
Zhang, G.Z., Liu, D.Y., He, X.L., Yu, D.Y., Pu, M.J., 2017. Acid rain in Jiangsu province, eastern China: tempo-spatial variations features and analysis. Atmos. Pollut. Res. 8, 1031–1043.
Zhang, Y.S., Zhao, H.B., Qian, L., Sun, M., Lv, X., Zhang, L., Petersen, J., Qiu, G., 2020b. A brief overview on the dissolution mechanisms of sulfide minerals in acidic sulfate environments at low temperatures: emphasis on electrochemical cyclic voltammetry analysis. Miner. Eng. 158, 106586.